RSC Advances

ROYAL SOCIETY OF CHEMISTRY

www.rsc.org/advances

Nitrogen-doped carbon sheets derived from chitin as non-metal bifunctional electrocatalysts for oxygen reduction and evolution

Haoran Yuan[a,c], Lifang Deng [a, c*], Xixi Cai[b], Shungui Zhou[b], Yong Chen[a,d], and Yong Yuan[b*]

[a]Guangzhou Institute of Energy Conversion, Chinese Academy of Sciences, Guangzhou 510640, China

[b]Guangdong Key Laboratory of Agricultural Environment Pollution Integrated Control, Guangdong Institute of Eco-Environmental and Soil Sciences, Guangzhou 510650, China;

[c]Key Laboratory of Renewable Energy, Chinese Academy of Sciences, Guangzhou 510640, China

[d]Guangzhou division Academy, Chinese Academy of Sciences, Guangzhou 510070, China

*** To whom Correspondence should be addressed:**

Email: denglf@ms.giec.ac.cn (F. Deng); Tel: 86-20-87013240; Fax: 86-20-87013240

Email: yuanyong@soil.gd.cn (Y. Yuan); Tel: 86-20-87025872; Fax: 86-20-87025872

Abstract

Affordable, efficient electrocatalysts for oxygen reduction reactions (ORR) and oxygen evolution reactions (OER) are critical for various energy technologies. Herein, we report that an activated carbon sheet (ACS) derived from chitin is an efficient non-metal bifunctional electrocatalyst for both ORR and OER. In alkaline media, the as-prepared ACS exhibited remarkable electrocatalytic activity for the oxygen reduction reaction, which was significantly superior to an unactivated carbon sheet (CS) and comparable to the commercial Pt/C catalyst with excellent durability and resistance to the crossover effect. Meanwhile, the same ACS also presents high catalytic activity towards OER, with a small overpotential of ~ 1.64 ± 0.02 V versus RHE. The excellent electrocatalytic properties of the ACS originated from the combined effect of optimal nitrogen doping, high surface area, and porous architecture. This work demonstrates that the ACS is a promising material candidate with high-performance in electrocatalytic applications in energy technologies.

Key words: activated carbon sheet; chitin; oxygen reduction reaction; oxygen evolution reaction; microbial fuel cell

Graphical abstract

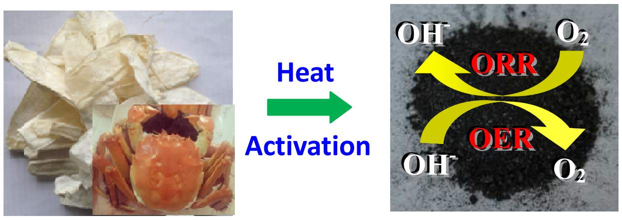

Highlight: Nitrogen-doped activated carbon sheets were derived from chitin, which exhibited remarkable activity for ORR and high catalytic activity towards OER.

1. Introduction

There is a growing interest in oxygen electrode catalysts, as conversions between O_2 and H_2O play a key role in a wide range of renewable energy technologies.[1,2] Oxygen reduction reactions (ORR) is the ubiquitous cathodes reaction in fuel cells and metal-air batteries and the current bottleneck for fuel cells lies in the sluggish kinetics of ORR, which causes severe energy efficiency loss, while oxygen evolution reactions (OER) is the anode reaction and plays a key role in energy conversion and storage such as solar fuel synthesis and rechargeable metal-air batteries. These two processes can be combined in a regenerative fuel cell, which represents as a promising energy storage device which works as a fuel cell and in reverse as a water electrollyzer to feed the fuel cell.[3, 4] However, both reactions are complicated by multi-electron transfer, leading to sluggish kinetics. To date, platinum (Pt)-based materials are the most widely used catalysts for ORR, but Pt has only moderate activity for OER. Ruthenium and iridium oxides are the best OER catalysts, but they are not as active as Pt for ORR.[5] On the other hand, these metals are both scarce and expensive and hence not practical for large-scale applications. Therefore, it is imperative to develop efficient and cost-effective electrocatalysts for both ORR and OER.

To date, various metal-free carbon materials that serve as the bifunctional electrocatalysts for both ORR and OER have attracted much attention due to their high catalytic activity, low cost, long durability, and abundance. For example, Tian et al. demonstrated that nitrogen-doped carbon-coated carbon nanotube (CNT) coaxial nanocables could be efficient catalysts for both ORR and OER.[6] Cheng et al. reported that boron-doped CNTs could catalyze both ORR and OER.[7] On the other hand, Lin et al. discovered that nitrogen-doped graphene prepared by pyrolysis of graphene oxide with polypyrrole also efficiently catalyzed both ORR and OER.[8] However, these metal-free carbon catalysts are mainly based on heteroatom-doped carbon nanotubes and graphene. The preparation of heteroatom-doped carbon nanotubes and graphene are currently still costly and involve complex synthetic steps and face the challenge of large-scale production to scale up for usage in fuel cell (FCs) systems. Recently, directly achieving heteroatom-doped carbon materials from natural resources has been reported to be a potential alternative to synthesized carbon materials for use as electrocatalysts. For example, Song et al. described seaweed-derived porous carbon as efficient for ORR.[9] Other natural materials (e.g., *Typha orientalis*, amaranthus, and ginkgo leaves) have also been reported as capable of being converting into high-performance electrocatalysts.[10,11] However, there is concern about the ORR activity of these materials and an extra annealing process in an NH_3 atmosphere is usually adopted to increase the N content in the as-prepared carbon materials.[11] Limited studies have been made to directly convert natural biomass into highly active electrocatalysts for both ORR and OER activity.

Chitin is the most abundant nitrogen-bearing compound in nature and the second-most abundant biopolymer on earth after cellulose and is extracted from shrimp, crab, crayfish and krill shells after their consumption as food.[12] Due to its renewable and biodegradable character, extremely small size, low density, chemical stability, biological activity, and noncytotoxicity, chitin is extensively used in medical applications,[12] nanocomposite fields,[13] and water treatment.[14] Moreover, a literature search revealed that chitin is suitable for converting into carbon materials with high porosity, which can be used as supercapacitor electrode materials. For instance, Nguyen et al. reported the pyrolysis of chitin with a designed nanorod structure to obtain a mesoporuos nitrogen-doped carbon material for a supercapacitor.[15] Herein, a low-cost N-doped carbon sheet derived from chitin was prepared as a high-efficiency ORR/OER catalyst. To increase its electroactivity, the carbon was chemically activated with $ZnCl_2$. When utilized as a metal-free electrocatalyst for ORR, the activated chitin-based carbon sheet exhibited comparable catalytic activity and enhanced long-term stability in comparison with a commercial Pt/C catalyst in a microbial fuel cell (MFC) system. On the other hand, the ACS also showed excellent activity for catalyzing OER.

2. Experimental

2.1 Preparation of activated carbon sheet from chitin

The chitin-derived carbon was prepared by carbonizing the hydrothermal product of chitin (purchased from Shan dong, Wei fang), which has been reported elsewhere.[16] In brief, 5 g of chitin and 40 mL deionized water were placed in a commercial Teflon-lined autoclave with a capacity of 50 mL, and the autoclave was sealed and heated at 180 ºC for 12 h. The resulting hydrothermal carbonaceous solid was recovered and washed with ethanol and deionized water several times, dried in an oven at 60 ºC, and ground in an agate mortar. Subsequently, the carbonaceous solid was thermo treated at 750 ºC for 2 h (dwell time) at a heating rate of 5 ºC/min in a tube furnace under an inert atmosphere to obtain unactivated chitin-based carbon sheet (CS). Activated chitin-based carbon sheet (ACS) was obtained by physically mixing $ZnCl_2$ with CS using an activating agent/carbon ratio of 3/1 (g/g) and then thermo treating under the same conditions as the CS preparation (Fig. 1A).[17] After cooling the excess zinc chloride present in the carbonized material was leached out by immersing in 1 mol/L HCl solution or 6 mol/L HCl and magnetic stirring for about 24 h in an oven at 80℃. Then the materials were extensively washed with water to get rid of traces of HCl and $ZnCl_2$, filtered and dried at 105 ºC. The metal impurities of the treated ACS materials were detected by inductively coupled plasma mass spectrometry (ICP-MS) (NexION-300).

2.2 Preparation of ACS cathodes and MFC operation

An air cathode was constructed as previously proposed by Yuan et al.[18] MFC chambers were cylindrical with an inner volume of 12 mL, with a water-proof and catalytic layer coating both sides of a wet-proof carbon cloth; the surface area of both the anode and cathode was 7 cm^2. The catalytic layer was prepared by mixing 50 mg ACS or 20 mg Pt/C (10%, Pt loading, HESEN, China) with 30 μL water, 5 μL Nafion solution (5% wt Sigma-Aldrich) and 50 μL ethanol, and the mixture was ultrasonicated for approximately 15 minutes to prepare a homogenous catalyst ink mixture. The obtained slurry was painted on one side of the air cathode using a brush and dried overnight at room temperature.

The culture media in the MFCs were 1 g/L sodium acetate solution in 50 mM phosphate buffer containing 12.5 mL/L mineral solution and 5 mL/L vitamin solution. MFCs were operated in batch mode with 1 kΩ external resistance. After stable voltage outputs were achieved, power density curves were obtained by changing the circuit resistor from 10000 Ω to 50 Ω, and individual electrode potentials were measured *vs.* a saturated calomel electrode (SCE). All tests were conducted in batch mode in a 30ºC incubator. The power was normalized by the projected surface area of the anode. All tests were conducted in triplicate, and the mean values are presented here.

2.3 Physical characterization

X-ray power diffraction (XRD, X'Pert-PRO, PANalytical, Netherlands) analysis was performed with a Cu Kα target (λ= 0.154056 nm) radiation source. SEM was conducted with a field emission scanning electronic microscope (FE-SEM, Model S-4800, Hitachi Ltd., Tokyo, Japan). XPS was performed using energy-dispersive X- ray spectroscopy (EDX, INCA 300). The specific surface areas were measured by the Brunauer-Emmett-Teller (BET) method, in which N_2 adsorption was applied at 77 K and a Carlo Erba Sorptometer was used.

2.4 The Electrochemical measurement

The electrochemical measurements were carried out in 0.1 mol/L KOH at room temperature using a CHI 605C electrochemical workstation (CHI Inc., USA). A Pt wire and a SCE were used as the counter and reference electrodes, respectively, and the catalysts coated glassy carbon (GC, 5.0 mm diameter) electrodes/rotating disk electrode were used as working electrodes. To prepare the working electrode, 2.0 mg of the prepared catalyst was mixed with 10 μL Nafion solution (5% Nafion) and 1 mL ethanol. The mixture was sonicated and 20 μL suspensions were then applied on glassy carbon and then fully dried. Prior to cyclic voltammogram (CV) scans, O_2 (or N_2) was bubbled through the electrolyte solution for 30 min to create an aerobic (or anaerobic) environment. ORR measurements were performed from 0.2 V to − 0.8 V, and OER measurements were performed from − 0.2 V to 1.0 V. For the purposes of comparison, commercial Pt/C (20 wt% platinum on carbon) was tested following the same procedure. The impedance of each MFC equipped with various cathodes was measured by electrochemical impedance spectroscopy (EIS) over a frequency range of 1×10^5 to 0.1 Hz with sinusoidal perturbation amplitude of 5 mV. The ohmic resistance (R_s) was obtained from the Nyquist impedance plots at the point where Z" was equal to zero at high frequency. The charge-transfer resistance (R_{ct}) for each MFC was estimated from a semi-circular fit of the charge-transfer impedance in the Nyquist plots.

3. Results and Discussion

3.1 Morphology and crystal structure

The surface morphology of the prepared samples was analyzed by the field scanning electron microscope (SEM) and is shown in Fig. 1 B, C, D and E. The SEM micrographs show that the chitin-based carbon had sheet morphology and composed of different porous structures. It seems that the chitin-based carbon after chemical activation (ACS) contained more and bigger cracks than the unactivated chitin-based carbon (CS). In addition, the Brunauer-Emmett-Teller (BET) surface areas are significantly different. ACS exhibits a surface area of 300.7 cm^2/g and a total pore volume of 0.31 cm^3/g, which was significantly larger than those of CS with a surface area of 100.0 cm^2/g and a total pore volume of 0.06 cm^3/g (Fig. 1F and G). The pore size distribution (Fig. 1G) calculated from the adsorption branches of the isotherms using

Barrett–Joyner–Halenda method reveals the presence of relatively uniform mesopores with the same centered pore diameter of 3.81 nm in both samples. However, a wider pore-size distribution was observed for ACS compared to CS. The increased BET surface area, total pore volume and pore-size distribution of ACS can be attributed to the chemical activation treatment, which is a very efficient method to obtain activated carbon from natural materials with high surface area and micro-pore distribution.[17] The chemical activation with $ZnCl_2$ is a redox reaction between chitin-based carbon and $ZnCl_2$; $ZnCl_2$ gets intercalated into the carbon matrix by impregnation then alter the pyrolysis behavior of carbon precursor. Upon pyrolysis, the impregnated $ZnCl_2$ causes dehydration of the carbon precursor leading to charring and aromatization along with the creation of pores. During the process of activation, liquid $ZnCl_2$ is formed above the melting point of $ZnCl_2$ (556 K), and which is mobile. Further increase in the temperature of activation, beyond the boiling point of $ZnCl_2$ (1003 K), interaction between carbon atoms and Zn species takes place resulting in a significant widening of the interlayers of carbon creating pores in the carbon matrix. During such severe interaction with carbon, $ZnCl_2$ aids removal of water from carbon structure by stripping off hydrogen and oxygen of the carbon precursor,[19] which causes a high portion of micro-pores. All of the above indicated that chemical activation plays a critical role in the preparation of carbon materials with larger specific surface areas and larger micro-pores and also hinted at their different electrochemical performance. However, chemical activation does not seem to exert any significant influence on the crystal forms of the carbon materials, with both XRD patterns of CS and ACS showing five broad peaks (Fig. S1) at 2θ of approximately 38º, 44º, 65º, 72º and 78º, revealing the amorphous nature of the prepared carbon materials.

With reference to functionality grafting, XPS is one of the surface analytical techniques that can provide useful information on the nature of the functional groups. The inset table in Fig. 2 provides the summary of element compositions of different samples determined by XPS. The ACS has a higher oxygen and nitrogen concentration than the CS. the XPS C 1s (284.78 eV), N 1s (400.88 eV) and O 1s (532.65 eV) peaks and some of the corresponding spectra of the prepared ACS material are presented in Fig. 2. Deconvolution of the C 1s spectrum of ACS (Fig. 2B) showed the main peak of graphite (284.77 eV) and two Gaussian peaks centered at 286.04 and 289.72 eV. The main peak at 284.77 eV originates in both sp^2-hybridized graphite-like carbon atoms and in carbon atoms bound to hydrogen atoms, which is observed in amorphous carbons, and their relative intensity correlates with the degree of graphitization.[20] Peaks with higher binding energies located at 286.04 and 289.72 eV are considered to originate in carbon atoms bound to nitrogen atoms or oxygen atoms, respectively.[21] The bonding energy of O 1s at 532.07 and 533.54 eV (Fig. 2C) was assigned to O=C and O-C bonds, respectively, which confirmed the presence of some carboxylic and hydroxyl groups on the ACS.[22] The complex XPS N 1s spectra (Fig. 2D) were fitted to three components of the binding energy, including pyridinic-N (398.20 eV), pyrrolic-N (399.40 eV) and graphitic-N (400.80 eV).[23,24] Among them, pyridinic-N is a nitrogen atom that bonds to two carbon atoms on the edge of a carbon plane and a carbon vacancy that is capable of adsorbing molecular oxygen and its intermediates in an oxygen reduction reaction. Meanwhile, pyridinic-N contributes one p-electron to the aromatic π-system and has a lone electron pair in the plane of the carbon matrix.[21] This will increase the electron-donating ability of the catalyst, thus promoting the electrocatalysis of the oxygen reduction reaction. In addition, as shown in Fig. S2 and Fig. S3, the XPS spectrum for the CS material is very similar to the ACS material, but the fractions of nitrogen groups are different, especially the fractions of pyridinic-N in the ACS (3.2%), which were higher than that in the CS (2.7%), and pyridinic-N was active for electrocatalysis of the oxygen reduction reaction. Therefore, the prepared ACS with high nitrogen content, high pyridinic-N fraction and porous structure leads to more active sites for the facilitation of oxygen reduction, which may result in higher electrocatalytic activity in ORR.

3.2 ORR activity of ACS electrocatalysts

Fig. 3A presents the CVs of Pt/C, ACS and CS supported glass carbon electrodes in 0.1 mol/L KOH solution with O_2 *vs.* N_2-saturation, and all data were recorded by cycling the potential at a scan rate of 10 mV/s until reproducible CVs were obtained. In the N_2-saturated solution, featureless voltammetric currents within the potential range between 0.2 V and −1.0 vs. SCE can be observed either for ACS or CS samples. In contrast, both the samples demonstrated well-defined cathodic peaks for O_2 reduction when the electrolyte solution was saturated with O_2, which is attributed to the electrocatalytic reduction of oxygen on the electrode. Remarkably, the ACS samples showed a positive peak potential at −0.24 V vs. SCE, and this activity can be assigned to nitrogen-doping in the prepared carbon, according to a previous study.[25] In addition, the chemical activation increased the surface area, in particular, adding surface functional groups and active sites onto the as-prepared material,[26,27] which can be the dominant control on electrochemical activities by the ACS. Then, ACS obtained higher cathodic currents than CS (Table S1).

To explore the ORR mechanism on the ACS and CS electrodes, rotating disk electrode (RDE) measurements were performed using various rotation speeds from 500 to 2000 rpm. The resulting I-V curves showed that the limited current density increased with increasing rotation speeds, suggesting that the diffusion distance was smaller at high speeds. The ORR polarization curves of the Pt/C, ACS and CS were recorded in O_2-saturated 0.1 M KOH at room temperature at a scan rate of 10 mV/s (Fig. 3B). The onset potential of the ACS (at about −0.15 V vs. SCE) was close to that of commercial Pt (at about −0.13 V vs. SCE) and was approximately 70 mV more positive than that of CS and considerably superior to most other reported carbon-based cathode catalysts (Table S2). The corresponding Koutecky-Levich (K-L) equations of the samples were applied to analyze the kinetic parameters including the electron-transfer number (n) and kinetic current density (j_k):[28]

$1/j=1/j_k+1/B\omega^{1/2}$ (1)

$B=0.2nFC (D)^{2/3}\nu^{-1/6}$ (2)

where j is the measured current density, j_k is the kinetic limiting current density, 1/B is the Levich slope, ω is the rotation speed, n is the total number of electrons transferred during the ORR, F is the Faraday constant, C is the bulk O_2 concentration in the electrolyte, D is the O_2 diffusion coefficient, and ν is the kinematic viscosity of the electrolyte. In the K-L plots of the electrodes, the relationship between 1/j and $\omega^{-1/2}$ was linear between – 0.5 V and – 0.8 V, then j_k and n was calculated from the slops and intercept of their linear fit lines (Fig. 3B). The j_k values at -0.7 V are 20.0 mA/cm^2 for ACS, which is significantly superior to that of CS (4.3 mA/cm^2), and only slightly lower than that of Pt/C (25 mA/cm^2) (Fig. 3C and D). To qualify the ORR processes on ACS and CS, Fig.1E and Fig. S4 shows four linear K-L plots based on the reaction current density on the LSVs at various rotating speeds, which suggested first-order reaction kinetics toward the concentration of O_2 for ACS, CS and Pt/C from -0.5 to -0.8V. Note that there is no well-defined diffusion limiting current plateau for all carbon samples, which is similar to other non-metal carbon-based catalysts for ORR.[29] This phenomenon resulted from the complicated mass transport process due to the presence of a rather thick film on the disk and the complex rough surface of the carbon-based catalysts. In addition, the electrocatalytic active sites of the catalysts are not homogenously distrusted, which can also result in the inclined current response to polarization.[30] The electron transfer number (n) of ACS was calculated as 3.87-3.99 at potentials ranging from -0.5 to -0.8 V, which was comparable to the number of electrons transferred by Pt/C under various potentials (Fig. S4A and 4B), indicating a four-electron process toward ORR on the ACS. However, the electron transfer number of the CS was calculated as 3.42-3.78, suggesting that the CS involves mixed four-electron and two-electron reduction processes with H_2O_2 as the intermediate agent (Fig. S4C and 4D). Clearly, the positive shift in the onset potential and enhancement in the ORR reduction current on the ACS electrode indicated that the ACS exhibited excellent catalytic activity, suggesting that chemical activation does contribute to lowering the overpotential of the ORR. However, metal impurities contained in original chitin should also be considered as factors that affect ORR activity because metallic impurities are often considered as the possible active center for ORR. According to previous reports, an optimal metal content of 0.2-4 wt% in carbon materials have been considered to involve in the catalytic reaction for the oxygen reduction.[31,32] However, as detected by ICP-MS, the ACS contains very low contents (0.0002 ~ 0.03% wt%) of Fe, Cu, Co and Ni impurities (Table S3). Moreover, the ACS with lower contents of impurities was obtained from the treatment by 6 M HCl than that from the 1 M HCl (Table S3). However, the similar catalytic activities for the ORR were achieved from these two ACS materials (Fig. S5). The above-mentioned results demonstrated that the metal impurities unlikely contributed towards the catalytic activity of the ACS for ORR. Besides, possible release of Pt from the counter electrode may contribute to the catalytic activity of the developed catalyst for the ORR. A two-compartment electrochemical cell was designed to avoid the interference of Pt dissolved from the counter electrode (Fig. S6A). As shown in Fig. S6B, the ACS still showed comparable activity for the ORR to the Pt/C in this two-compartment electrochemical cell, which ruled out the possible effect of the released Pt from the counter electrode on the measured catalytic activity of the ACS. Moreover, the metal impurities in electrolyte before/after ORR measurements were also detected by ICP-MS (Table S4). Extremely low contents of metal impurities were examined in the electrolytes, which eliminated the possible effect of the metal impurities in the electrolyte on the catalytic activity of the ACS. However, it is worth mentioning that possible effects of metal impurities on the observed excellent ORR performance of the ACS could still be a matter of controversy unless absolutely metal-free N-doped carbon materials could be produced from chitin.

3.3 Performance of ACS cathode in MFCs

Microbial fuel cells (MFCs) are capable of using wastewater as anodic “fuel” to generate electricity and accomplish pollutant treatment simultaneously.[33] However, the prohibitive cost, scarcity and low stability of Pt hampered the large-scale commercialization of these technologies.[34] To further demonstrate catalytic capability for the ORR and the stability of the ACS, the ACS was applied in MFCs as the cathode catalyst. For comparison, a Pt/C catalyst is used as benchmark control. After the cell voltages were stabilized, the cell voltage curves, anode and cathode polarization curves, and power density curves were evaluated. As shown in Fig. 4A, the maximum power density of the MFC with the ACS catalyst air cathode is 705 ± 5 mW/m^2, which is much higher than that of the CS catalyst air cathode (474 ± 5 mW/m^2) and comparable to that of the Pt/C cathode (727 ± 5 mW/m^2). This result suggests that the ACS cathode performs high catalytic activity and improves the power generation. Curves of the individual cathode or anode potential versus current density are shown in Fig. 4B. The anode potentials of the MFCs with different cathodes have few differences, while the cathode potentials are greatly different, indicating that the differences in the MFC performances mainly resulted from the variations in the catalytic activities of the cathode catalysts.

The power outputs of MFCs were related to the measured impedance values (Fig. S7A and Table S1). Due to the identical anode configuration in all MFCs, the varied impedance values should result from the cathodes. The Nyquist plots were measured on the electrodes with different catalysts. All the Nyquist plots of the electrode with different catalysts intercept the real axis and the diameter of the first semicircle in the spectra over the high-frequency to obtain the ohmic (R_s) and charge-transfer resistances (R_{ct}). The

MFC with the CS cathode had the highest impedance ($R_s = 49 \pm 2\ \Omega$ and $R_{ct} = 45 \pm 3\ \Omega$), which was higher than that of the ACS cathode ($R_s = 48 \pm 2\ \Omega$ and $R_{ct} = 35 \pm 2\ \Omega$). For the ACS and CS cathodes, the R_s values are identical but a little higher than the Pt/C cathode ($R_s = 36 \pm 2\ \Omega$). However, the value of R_{ct} for the ACS was comparable to the Pt/C ($31 \pm 3\ \Omega$) cathodes. Because a faster electron-transfer rate could be indicated by a smaller R_{ct}, the low R_{ct} of the ACS electrode suggested an improved electron transfer resistance and increased reaction rate compared to the CS electrode. This result could be explained by the greater catalyst surface area and more active sites of the ACS.

The long-term operation of the MFCs was studied to evaluate the stability of the prepared catalysts. Approximately 60 full discharging – charging cycles with 1 kΩ external loading were tested. As shown in Fig. 4C and 4D, the output of the MFC with the Pt/C cathode decreased to only 73% of the initial voltage after 60 days, which was much lower than that of the ACS (97%) and CS (96%), suggesting that the prepared catalysts had outstanding stability in the MFCs. In addition, the MFC with the Pt/C cathode had the highest voltage output at the beginning, but it decreased significantly and became lower than the ACS or CS approximately 20 and 40 days later, respectively, demonstrating that the ACS catalyst can be a potential alternative to Pt/C in MFCs for sustainable energy generation. Moreover, the ORR performance of Pt/C is substantially diminished due to the crossover of substrates and metabolites that results in the formation of mixed potentials and the flow of internal currents.[35] As shown in Fig. S7B, the ORR amperometric current of the Pt/C electrode was significantly affected by the addition of methanol. However, the ACS electrode current was not affected, demonstrating that the crossover effect was smaller in the ACS, and therefore, the ACS were more stable in the fuel cell. It is believed that the prepared carbon shows several advantages as the electrocatalysts for ORR. First, the cost of the ACS catalyst is ultra-low. Second, the prepared ACS catalyst showed high activity, improved kinetics and excellent stability in the MFC environment.

3.4 OER activity of ACS electrocatalysts

Apart from the ORR activity, excellent OER activity is also achieved with the ACS. To study the electrocatalytic activity of the as-prepared catalyst in OER, a three-electrode system with polarization experiments with the potential extended to the water oxidation regime (from –0.2 to 1.0 V) was used. To examine the onset of the electrocatalytic OER, LSVs of the catalysts are shown in Fig. 5 with a sweep rate of 10 mV/s. As seen in the LSVs, the catalytic current was observed at approximately 0.05 V, 0.63 V and 0.61 V vs. SCE (approximately 1.06 V, 1.64 V and 1.62 V vs. RHE) for the activated chitin-based carbon (ACS), unactivated chitin-based carbon (CS) and Pt/C catalysts, respectively, and its OER current density at 1.0 V reached – 20.7, – 3.9 and – 12.4 mA/cm^2, respectively. The OER activity on the CS is quite faint, while excellent OER activity of the ACS catalyst was observed, which is much more active than other carbon-based materials (Table S2). Furthermore, as reported by Zhao et al., the potential required to oxidize water at the current density of 10 mA/cm^2 is usually used to judge the OER activity.[36] The ACS catalyst generated a current density of 10 mA/cm^2 at a current of 0.64±0.02 V versus SCE (approximately 1.64 ±0.02 V versus RHE), which is similar to that of IrO_2/C materials (10 mA/cm^2, 1.60 ±0.01 V versus RHE) and nitrogen-doped graphene/single-walled CNT hybrids.[36] However, the CS afforded a current density of 10 mA/cm^2 at a much higher overpotential than that of the ACS, implying the superior OER activity of ACS due to chemical activation. As for the Pt/C, the potential acquired for the current density of 10 mA/cm^2 would be much more positive, as deduced from the corresponding current trend. The Tafel slope for the ACS catalyst was approximately 90 mV/decade (Fig. 5B), much smaller than that of the CS (116 mV/decade) and the commercial Pt/C (104 mV/decade), which further confirmed the superior electrocatalytic OER performance of ACS. N-doped non-metal carbon materials have been demonstrated to be active for the OER. For instance, Zhao et al. revealed that nitrogen-related species is the active centre of OER activity, and with the increasing levels of pyridinic-N and quaternary-N, the OER activity of the N/C catalyst improved.[36] As shown in the inset table of Fig. 1 and in Fig. S3, the N-content (4.99%) and specific surface area (300.7 m^2/g) of the ACS were higher than those of the CS (3.69%, 106.4 m^2/g), especially the fractions of pyridinic-N in the ACS was about 3.2%, which may the main reason for the resultant high OER activity of the ACS material.

4. Conclusions

In conclusion, the CS and ACS were successfully fabricated from chitin by a facile and cost-favorable heat treatment, and their electrochemical characteristics were investigated to determine their potential use in energy technologies. The prepared ACS possess large surface area, high nitrogen content and porous structure, leading to more active sites for the facilitation of oxygen reduction, which was superior to the CS and comparable to the commercial Pt/C catalyst with excellent durability and resistance to the crossover effect in an alkaline electrolyte. We also found that the ACS presented high catalytic activity towards OER. This work provides a platform towards the design of simple, inexpensive and non-metal materials with extraordinary electron pathways that can be used as high–performance bifunctional oxygen electrode activity for both ORR and OER.

Acknowledgements

We gratefully acknowledge financial support from Guang dong Natural Science Funds for Distinguished Young Scholar (2014A030306033), the National 973 project of China (2011CB201501), Pearl River Nova Program of Guangzhou (2013J2200008), and National Natural Science Foundation of China (No.51406207).

References

[1] M. Winter, R.J. Brodd, *Chem. Rev.* 2004,**104**,4245-4269.

[2] A.A. Gewirth, M.S. Thorum, *Inorga. Chem.* 2010,**49**,3557-3566.

[3] W. L. Yao, J. Yang, J. L. Wang, Y. N. Nuli, *Electrochem. Commun*. 2007,**9**,1029-1034

[4] S. D. Song, H. M. Zhang, X. P. Ma, Z. G. Shao, Y. N. Zhang, B. L. Yi, *Electrochem. Commun*. 2006,**8**,399-405

[5] S. Trasatti, *Electrochim. Acta.* 1984,**29**,1503-1512.

[6] G.L. Tian, Q. Zhang, B. Zhang, Y.G. Jin, J.Q. Huang, D.S. Su, F. Wei, *Adv. Funct. Mater.*. 2014,**24**, 5956-5961.

[7] Y.H. Cheng, Y.Y. Tian, X.Z. Fan, J.G. Liu, C.W. Yan, *Electrochim. Acta*. 2014,**143**,291-296.

[8] Z.Y. Lin, G.H. Waller, Y. Liu, M.L. Liu, C.P. Wong, *Carbon*. 2013,**53**,130-136.

[9] M.Y. Song, H.Y. Park, D.S. Yang, D. Bhattacharjya, J.S. Yu, *ChemSusChem.* 2014,**7**, 1764-1764.

[10] P. Chen, L.K. Wang, G. Wang, M.R. Gao, J. Ge, W.J. Yuan,Y.H. Shen, A.J. Xie, S.H. Yu, *Energy Environ. Sci.* 2014,**7,** 4095-4103.

[11] F.P. Pan, Z.Y. Cao, Q.P.Zhao, H.Y Liang, J.Y Zhang, *J. Power Sources*. 2014, **272**, 8-15.

[12] A.M. Salaberria, S.C.M. Fernandes, R.H. Diaz, J. Labidi, *Carbohydr. Polym.* 2015,**116**,286-291.

[13] J.B. Zeng , Y.S. He, S.L. Li, Y.Z. Wang, *Biomacromolecules*. 2012,**429**,1-11.

[14] P.K. Dutta, J. Dutta, V. Tripathi, *J. Sci. Ind. Res.* 2004,**63**, 20-31.

[15] T.D. Nguyen, K.E. Shopswitz, M.J. Maclachlan, *J. Mater. Chem. A*. 2014,**2**,5915-5921.

[16] H.R. Yuan, L.F. Deng, Y.J. Qi, N. Kobayashi, J.H. Tang, *J. Sci. World.* 2014,**2014**, 1-8.

[17] X.J. Liu, L.G. Li, W.J. Zhou, Y.C. Zhou, W.H. Niu, S.W. Chen, *Chemelectrochem.* 2015,**4**,1-9.

[18] Y. Yuan, J. Ahmed, S. Kim, *J. Power Sources.* 2011,**196**,1103-1106.

[19] Z.H. Hu, E. F. Vansant, *J. Colloid Interface Sci.* 1995,**176**, 422-431.

[20] A. Hiroki, K. Thomas, C. Franco, R.S. Willian, S.P.S. Milo, H.W. Alan, H.F. Richard, *J. Phys. Chem. B.* 1999,**103**,8116-8121.

[21] S. E. Baker, W. Cai, T. L. Kasseter, K. P. Weidkamp, R. J. Hamers. *Nano Lett*，2002, **2**, 1413-1417

[22] M. T. Martinez, M. A. Callejas, A. M. Benito, M. Cochet, *Carbon*, 2003, **41**,2247-2256.

[23]G. Liu, X. Li, P. Ganesan, B.N. Popov, *Appl. Catal., B: Environ.* 2009,**93**,156-165.

[24] Q. Wen, S. Wang, J. Yan, L. Cong, Y. Chen, H. Xi, *Bioelectrochem*. 2014,**95**,23-28.

[25] S. Mao, Z. Wen, T. Huang, Y. Hou, J. Chen, *Energy Environ. Sci.* 2014,**7**,609-615.

[26] Y.M. Zhou, B. Gao, A.R. Zimmerman, J. Fang, Y. Sun, X. Cao, *Chem. Eng. J.* 2013,**231**,512-518.

[27] Y.W. Xue, B. Gao, Y. Yao, M. Inyang, M. Zhang, A.R. Zimmerman, K.S. Ro, *Chem. Eng. J.* 2012,**200-202**, 673-680.

[28] I. Roche, E. Chaînet, M. Chatenet, J. Vondrák, *J. Phys. Chem. C.* 2007,**111**, 1434-1443.

[29] Y. L. Li, J.J. Wang, X.F. Li, D.S. Geng, M.N. Banis, R.Y. Li, X.L. Sun, *Electrochem. Commun.* 2012,**18**, 12-15.

[30] H. J. Zhang, X.X.Yuan, L.L. Sun, J.H. Yang, Z.F. Ma, Z.P. Shao, *Electrochim. Acta.* 2012,**77**,324-329

[31] C. W. B. Bezerra, L. Zhang, K. C. Lee, H. S. Liu, A. L. B. Marques, E. P. Marques, H. J. Wang and J. J. Zhang, Electrochim. Acta, 2008, 53, 4937–4951.

[32] Y. Li, W. Zhou, H. Wang, L. Xie, Y. Liang, F. Wei, J.-C. Idrobo, S. J. Pennycook andH. Dai, Nat. Nanotechnol., 2012, 7, 394–400.

[33]B.E. Logan, J.M. Regan, *Trends Microbiol.* 2006,**14**,512-518.

[34] R.A. Rozendal, H.V. Hamelers, K. Rabaey, J. Keller, C.J. Buisman, *Trends biotechnol.* 2008,**26**, 450-459.

[35] F. Harnisch, S. Wirth, U. Schröder, *Electrochem. Commun.* 2009,**11**, 2253-2256.

[36] Y. Zhao, R. Nakamura, K. Kamiya, S. Nakanishi, K. Hashimoto, *Nature commun.* 2013,**4**,2390-2396.

Figure captions

Figure 1. SEM images of the as-prepared carbon materials: (B and D) CS; (C and E) ACS (D and E are higher magnification images of CS and ACS, respectively); (F and G) pores distribution of CS and ACS

Figure 2. A) XPS survey of the ACS showing C, O and N as the main elements; B) The XPS C 1s spectra; C) O 1s spectra; D) N 1s spectra

Figure 3. (A) CVs of electrodes with different catalysts in O_2- or N_2-saturated 0.1 M KOH; (B) RDE voltammograms of the CS, ACS and Pt/C at 1500 rpm; (C) K-L plots at -0.7 V from ACS, CS and Pt/C D) Electrochemical activity given as the kinetic current (j_k) at -0.7 V for ACS, CS and Pt/C. E)RDE voltammograms of the ACS in O_2-saturated 0.1 M KOH collected with a sweep rate of 10 mV/s at various rotation speeds; (F) corresponding Koutecky-Levich plots (j^{-1} *vs.* $\omega^{-0.5}$) at different potentials on the ACS electrode

Figure 4. (A) Polarization curves of MFCs with different cathodes; (B) individual potential (vs. SCE) vs. current density curves; (C, D) long-term stability tests of the MFCs (the voltage outputs were examined at 1000 Ω)

Figure 5. (A) OER current of Pt/C, ACS and CS electrode on 0.1 mol/L KOH solution at a scan rate of 10 mV/s. (B) Tafel plots derived from (A).

Figure 1

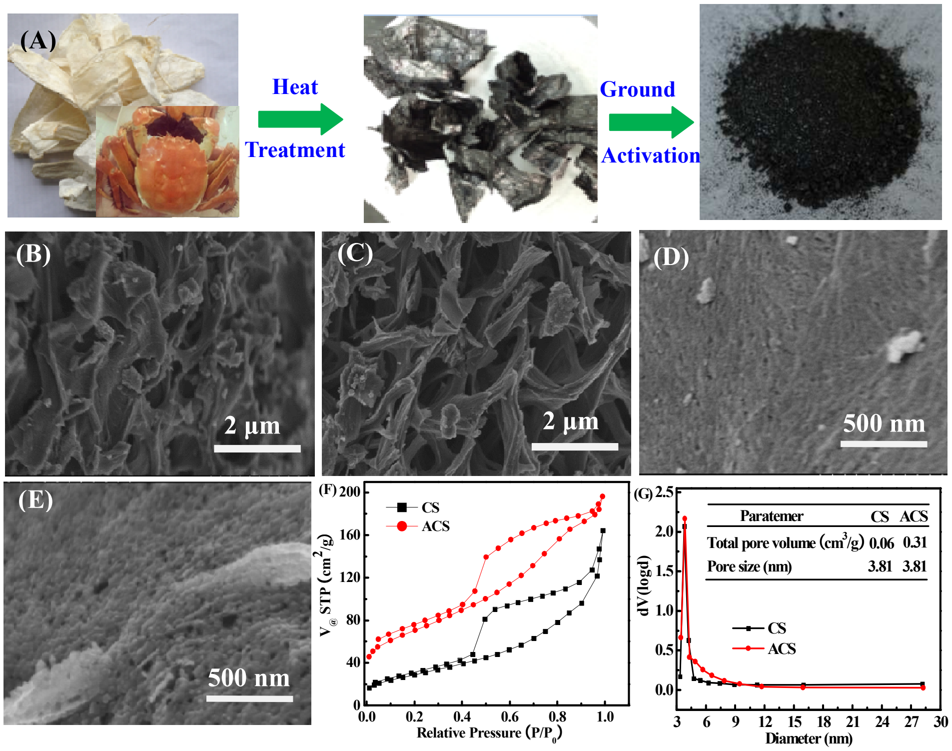

Paratemer	CS	ACS
Total pore volume (cm^3/g)	0.06	0.31
Pore size (nm)	3.81	3.81

Figure 2

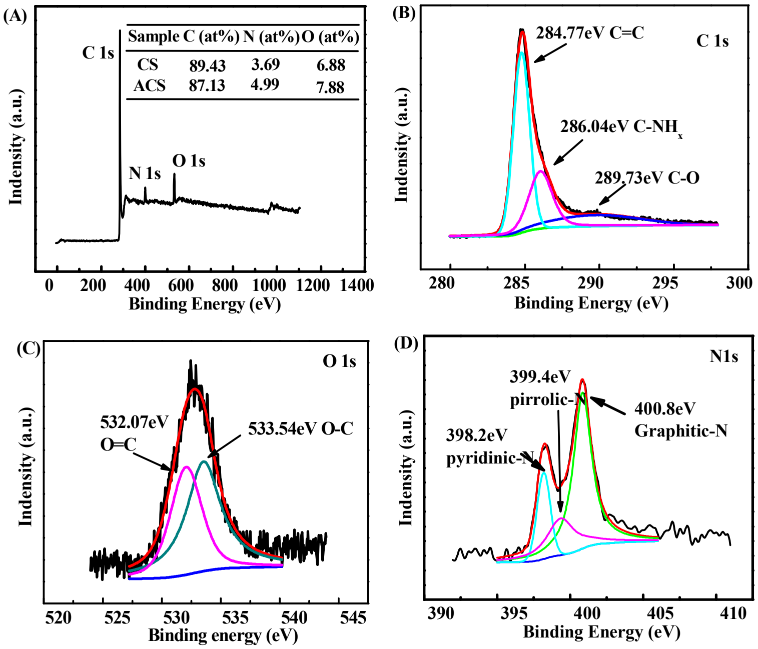

Sample	C (at%)	N (at%)	O (at%)
CS	89.43	3.69	6.88
ACS	87.13	4.99	7.88

Figure 3

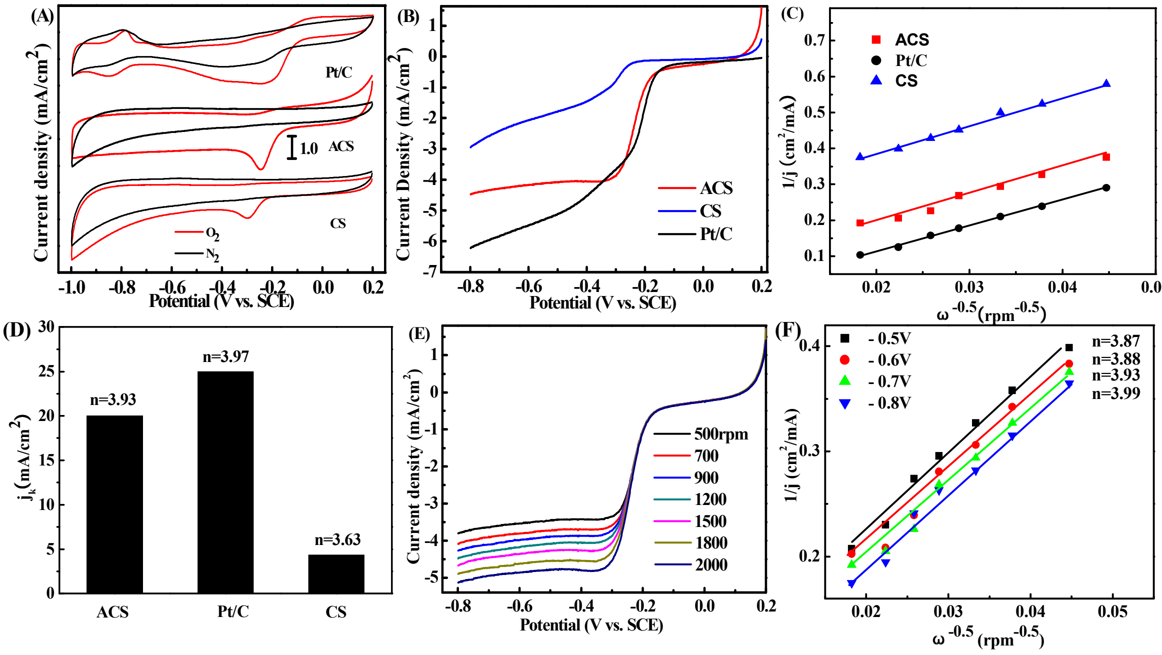
(A)
Current density (mA/cm^2)
Pt/C
1.0
ACS
CS
O$_2$
N$_2$
-1.0 -0.8 -0.6 -0.4 -0.2 0.0 0.2
Potential (V vs. SCE)
(B)
Current Density (mA/cm^2)
1 0 -1 -2 -3 -4 -5 -6 -7
ACS
CS
Pt/C
-0.8 -0.6 -0.4 -0.2 0.0 0.2
Potential (V vs. SCE)
(C)
1/j (cm^2/mA)
0.7 0.6 0.5 0.4 0.3 0.2 0.1
ACS
Pt/C
CS
0.02 0.03 0.04 0.05
ω$^{-0.5}$(rpm$^{-0.5}$)
(D)
j$_k$ (mA/cm^2)
30 25 20 15 10 5 0
n=3.93
n=3.97
n=3.63
ACS
Pt/C
CS
(E)
Current density (mA/cm^2)
1 0 -1 -2 -3 -4 -5
500rpm
700
900
1200
1500
1800
2000
-0.8 -0.6 -0.4 -0.2 0.0 0.2
Potential (V vs. SCE)
(F)
1/j (cm^2/mA)
0.4 0.3 0.2
- 0.5V
- 0.6V
- 0.7V
- 0.8V
n=3.87
n=3.88
n=3.93
n=3.99
0.02 0.03 0.04 0.05
ω$^{-0.5}$ (rpm$^{-0.5}$)

Figure 4

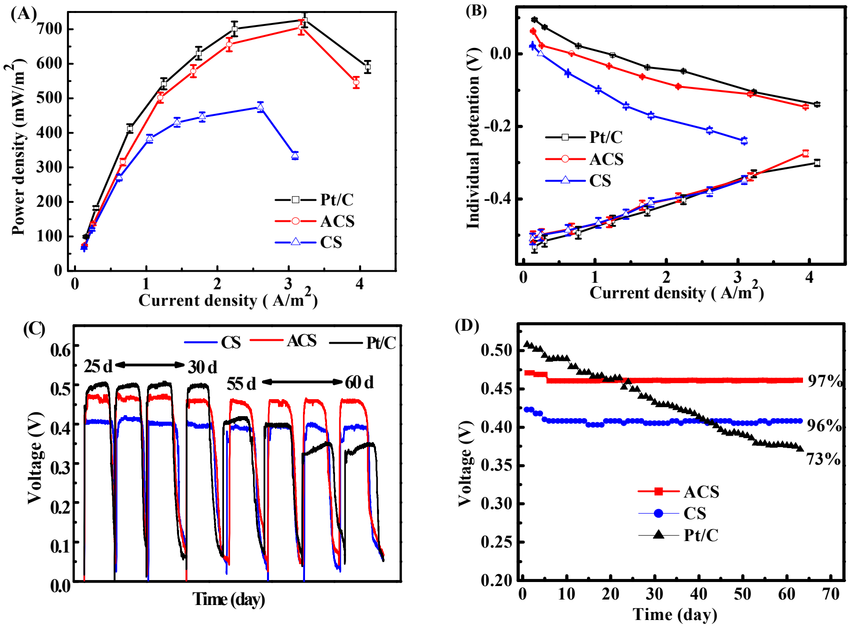
(A)
Power density (mW/m^2)
0
100
200
300
400
500
600
700
0
1
2
3
4
Current density (A/m^2)
Pt/C
ACS
CS
(B)
Individual potention (V)
0.0
-0.2
-0.4
0
1
2
3
4
Current density (A/m^2)
Pt/C
ACS
CS
(C)
Voltage (V)
0.0
0.1
0.2
0.3
0.4
0.5
0.6
CS
ACS
Pt/C
25 d
30 d
55 d
60 d
Time (day)
(D)
Voltage (V)
0.20
0.25
0.30
0.35
0.40
0.45
0.50
0
10
20
30
40
50
60
70
Time (day)
97%
96%
73%
ACS
CS
Pt/C

Figure 5

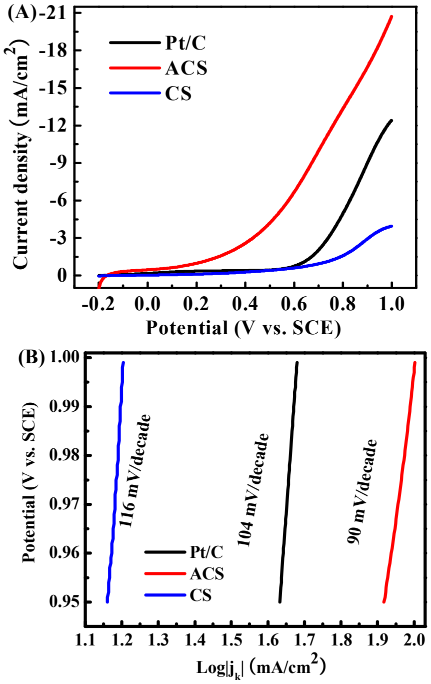
(A)
Current density (mA/cm^2)
-21
-18
-15
-12
-9
-6
-3
0
Pt/C
ACS
CS
-0.2
0.0
0.2
0.4
0.6
0.8
1.0
Potential (V vs. SCE)
(B)
Potential (V vs. SCE)
1.00
0.99
0.98
0.97
0.96
0.95
116 mV/decade
104 mV/decade
90 mV/decade
Pt/C
ACS
CS
1.1
1.2
1.3
1.4
1.5
1.6
1.7
1.8
1.9
2.0
Log|j$_k$| (mA/cm^2)